

## Tidally Torn: Why the Most Common Stars May Lack Large, Habitable-Zone Moons

SHAAN D. PATEL ,<sup>1</sup> BILLY QUARLES ,<sup>2</sup> NEVIN N. WEINBERG ,<sup>1</sup> AND MANFRED CUNTZ ,<sup>1</sup>

<sup>1</sup>*Department of Physics, University of Texas at Arlington  
 Arlington, TX 76019, USA*

<sup>2</sup>*Department of Physics and Astronomy, East Texas A&M University  
 Commerce, TX 75428, USA*

### ABSTRACT

Earth-like planets in the habitable zone (HZ) of M-dwarfs have recently been targeted in the search for exomoons. We study the stability and lifetime of large (Luna-like) moons, accounting for the effects of 3-body interactions and tidal forces using the N-body simulator `rebound` and its extension library `reboundx`. We find that those moons have a notably different likelihood of existence (and, by implication, observability). Large moons orbiting Earth-like planets in the HZs of M4 and M2 dwarfs become unstable well before  $10^7$  and  $10^8$  yr, respectively, and in most cases, those orbiting M0-dwarfs become unstable in much less than  $10^9$  yr. We conclude that HZ planets orbiting M-dwarfs are unlikely to harbor large moons, thus affecting the total number of possible moons in our galaxy and the Universe at large. Since moons may help enhance the habitability of their host planet, besides being possibly habitable themselves, these results may have notable implications for exolife, and should also be considered when seeking solutions to the Drake equation and the Fermi paradox.

*Keywords:* exoplanets – planets and satellites: dynamical evolution and stability – tides – habitable zone

### 1. INTRODUCTION

As the number of exomoon candidates increases, there is heightened interest in studies of exomoon formation, orbital stability, and habitability (R. C. Domingos et al. 2006; R. Heller et al. 2014; M. Rosario-Franco et al. 2020). Exomoon candidates include Kepler-1625b-i and 1708b-i (A. Teachey & D. M. Kipping 2018; D. Kipping et al. 2022, 2025). In both cases the host stars are solar type (G. D. Mulders et al. 2015), although there is no a priori reason exomoons could not exist around other types of stars (D. M. Williams et al. 1997; D. Kipping et al. 2022). Based on detailed evaluations of both the initial mass function (IMF) and present-day mass function (PDMF) of the Milky Way as well as other galaxies (P. Kroupa 2001, 2002; G. Chabrier 2003; Y.-T. Wang et al. 2025), M-dwarfs are considered the most frequent type of stars.

In recent years, the investigation of exomoons orbiting HZ planets and specifically within M-dwarf systems has garnered increasing attention (D. M. Kipping et al. 2013, 2014), making it crucial to examine the conditions necessary for exomoons to exist in such systems. Moreover, E. Pass et al. (2024) proposed for (and was awarded)

observations to search TOI-700d for a Luna-like moon analog orbiting the HZ terrestrial planet using the James Webb Space Telescope (JWST). A particular aspect of exomoons concerns objects situated in stellar habitable zones (HZs). Those are regions around a star at which liquid water could exist on a planetary or moon surface (J. F. Kasting et al. 1993; R. K. Kopparapu et al. 2013; J. F. Kasting et al. 2014; R. M. Ramirez 2018). HZs are also known as “Goldilocks zones,” where conditions might be just right for life based on the standard biochemical paradigm (W. T. Sullivan & J. Baross 2001).

Prominent scenarios of HZ exomoons include possible cases where such moons are hosted by Jupiter-type planets in distant HZs, potentially allowing habitability (D. M. Williams et al. 1997; L. Kaltenegger 2017), including HD 23079 (C. G. Tinney et al. 2002). Detailed dynamical studies identified regions of stability of HZ exomoons (M. Cuntz et al. 2013; O. Jagtap et al. 2021; S. D. Patel et al. 2025), including plausible tidal interactions within the system, which was found to be insufficient to induce significant outward migration toward the theoretical stability limit due to the large star–planet separation. However, previous studies suggest significant dynamical challenges. S. R. Kane (2017),

T. Trifonov et al. (2020), and S. D. Patel et al. (2025) found that strong perturbations and tidal effects generally prevent long-term moon survival in systems like TRAPPIST-1, GJ 1148, and K2-18, while H. Martínez-Rodríguez et al. (2019), using tidal evolution models, identified only a small subset of massive HZ planets where exomoons could remain stable for over 0.8 Gyr.

This study aims to assess the dynamical stability of exomoons within the HZs of M-dwarf stars through a comprehensive exploration of the parameter space for host planets with masses between 0.8 and 2.0 Earth masses, orbiting spectral types M0 to M4, while accounting for a range of tidal dissipation efficiencies<sup>3</sup>. Our methodology is based on a novel approach that enables us to determine tidal migration timescales by including N-body integrations along with tidal effects. Simulations will be given for M0, M2, and M4 candidate stars.

This dynamical concept expands on previous purely analytical approaches by leveraging the latest features of the `reboundx` library, including recent expansions. Sets of model calculations are pursued for planets at different locations in M-dwarf HZs assuming they host Luna-size moons. The orbital stability of those moons will be carefully assessed, which informs the kinds of systems that can be expected to exist in nature.

The Drake equation estimates the abundance of advanced civilizations in our galaxy by combining astrophysical and biological probabilities while the Fermi paradox highlights the contradiction between this expected abundance and the lack of evidence to date (F. Drake & D. Sobel 1993; M. J. Burchell 2006; D. Kipping 2021; G. M. Szabó et al. 2024; D. Kipping & G. Lewis 2025; M. Civiletti 2025). The possible scarcity of HZ moons around M-dwarfs could be a contributing factor to both.

Section 2 describes the methods used in this study, whereas Sect. 3 reports our results and discussion. Our summary and conclusions are given in Sect. 4, whereas Sect. 5 conveys an outlook of future observational concepts allowing to test our theoretical predictions.

## 2. METHODS

### 2.1. Numerical Simulation Setup

We employ the N-body integrator `rebound` (v4.4.3) (H. Rein & S. F. Liu 2012), in conjunction with the extension library `reboundx` (v4.3.0) (D. Tamayo et al.

<sup>3</sup> Contemporaneous with our work, Y. Su & M. Saillenfest (2025) focus on warm planets with orbital periods of 10-200 days and the potential in-fall after planetary spin-down. They use a classical approach that neglects the mean motion perturbations potentially affecting the putative moon.

2020), to examine the orbital stability of exomoons surrounding Earth-like planets within the HZs of M-dwarf systems, incorporating tidal effects. The `tides_spin` module (T. Lu et al. 2023) uses a constant time-lag tidal model that follows the prescription of tides (P. P. Eggleton et al. 1998). Our simulations use the TRACE integrator (T. Lu et al. 2024) along with the `IAS15` integrator (H. Rein & D. S. Spiegel 2015) to model close encounters between the host planet and the potential moon, with the initial integration timestep set to 20% of the moon's initial orbital period.

### 2.2. Habitable Zone Limits

To determine the inner and outer HZ distances for specific M-dwarf spectral types (M0, M2, M4), we apply Equation 5 from R. K. Kopparapu et al. (2014). We adopt the  $1.0 M_{\oplus}$  constants for the runaway greenhouse (inner HZ) and maximum greenhouse (outer HZ) limits using the temperature and luminosity values reported in M. J. Pecaut & E. E. Mamajek (2013); however, the selection of these constants is not expected to notably influence the resulting HZ boundaries. We use the inner and outer HZ distances as the range for our initial planetary semi-major axis values ( $a_p$ ) for an M0-dwarf (0.27 – 0.52 au), M2-dwarf (0.17 – 0.35 au), and M4-dwarf (0.08 – 0.18 au), with a step size of 0.001 au applied across all three cases; see Table 1 and Fig. 1 for details.<sup>4</sup>

### 2.3. Initial and Stopping Conditions

We investigate Earth-like host planets with a planetary mass between 0.8 and 2.0  $M_{\oplus}$ , stepping by 0.01  $M_{\oplus}$ . The planetary radius is kept at a constant  $1R_{\oplus}$  for all runs while the host star and moon remain point masses. For comparison, the mean radius of TOI-700d is only slightly larger ( $\lesssim 1.2R_{\oplus}$ ) than an Earth-radius (E. A. Gilbert et al. 2020, 2023). The planet begins with an Earth-like Love number ( $k_2 = 0.298$ ), moment of inertia constant ( $\bar{C} = 0.3308$ ), and time-lag ( $\tau_p = 698$  s) (O. Neron de Surgy & J. Laskar 1997; Bolmont, Emeline et al. 2015), while the planetary spin period begins at 5 hours, which is consistent with our current knowledge for the spins of protoplanets (E. Kokubo & H. Genda 2010; K. Takaoka et al. 2023). In all simulations, the mass of the moon ( $M_m$ ) equals that of Earth's moon, Luna, while the semi-major axis of the moon ( $a_m$ ) starts

<sup>4</sup> The computational cost of our longest running simulation is about 14 days, but the majority of the simulations finish within a 1-2 days where using a medium-large computing cluster makes the range of semi-major axis values tenable.

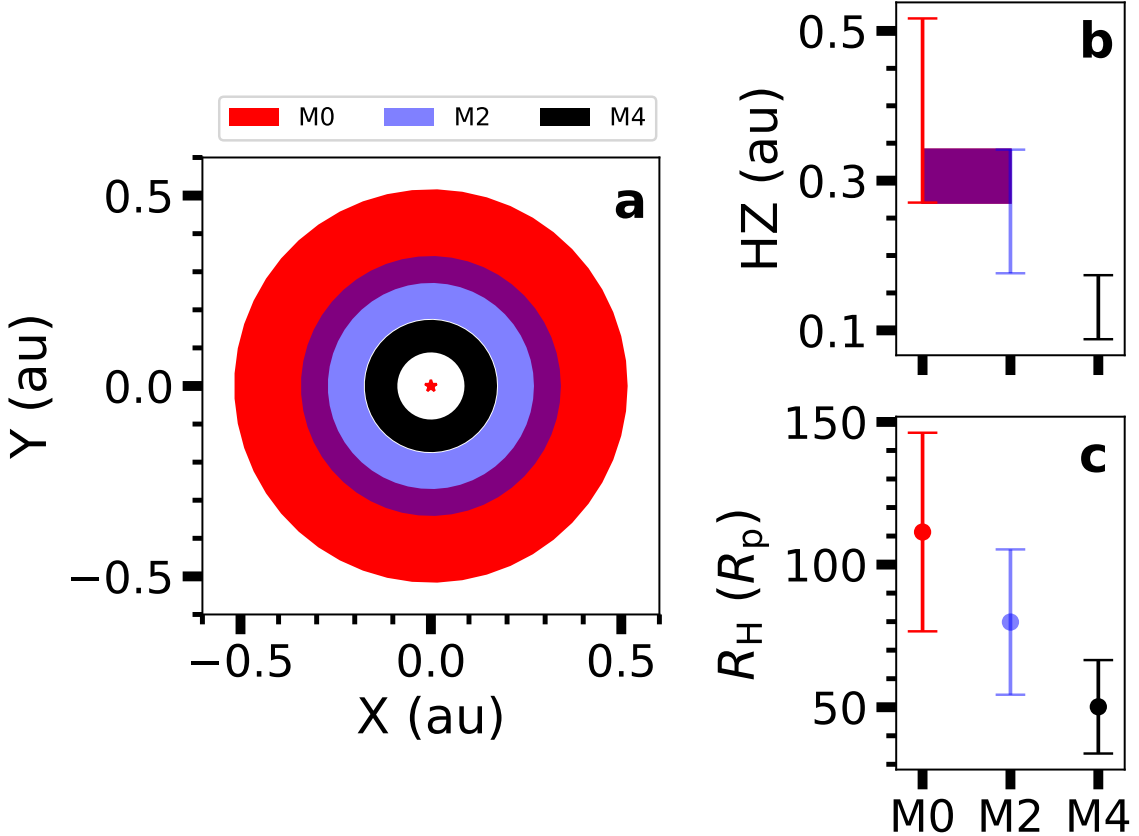


**Figure 1.** HZs and Hill Radii of M0, M2, and M4 stars. (a) Top-down and (b) edge-on views of the HZs around M0 (red), M2 (blue), and M4 (black) dwarfs along with (c) the Hill radius for a prospective  $1.0 M_\oplus$  planet at the center of its respective HZ. The overlap of the M0 and M2 HZs is noted in purple in both (a) and (b).

at  $3 \times$  the Roche limit of a fluid satellite, calculated by

$$R_{\text{Roche}} = 2.44R_p(\rho_\oplus/\rho_m)^{1/3}, \quad (1)$$

where  $\rho_\oplus$  and  $\rho_m$  denote the densities of the Earth ( $5.515 \text{ g cm}^{-3}$ ) and Luna ( $3.34 \text{ g cm}^{-3}$ ), respectively. See Table 1 for additional information. Numerical simulations of the Giant Impact Hypothesis show that Earth's moon likely formed just exterior to  $R_{\text{Roche}}$  (R. M. Canup 2004). The fastest outward migration occurs when the tides are strongest (i.e., near  $R_{\text{Roche}}$ ) so that starting a moon from  $1 - 3 R_{\text{Roche}}$  is somewhat arbitrary, where we make a fiducial choice. Each simulation evolves the star–planet–moon system up to 200 Myr, where a simulation is terminated if the moon's semi-major axis extends beyond the critical semi-major axis  $a_{\text{crit}}$ , defined as

$$a_{\text{crit}} = 0.4031(1 - 1.123e_p)R_H, \quad (2)$$

where  $e_p$  and  $R_H$  are the eccentricity and the Hill radius of the planet, respectively (M. Rosario-Franco et al. 2020).

R. C. Domingos et al. (2006) provided a more optimistic criterion ( $a_{\text{crit}} \approx 0.4895 R_H$ ) due to a bias in their starting conditions (see M. Rosario-Franco et al. 2020). Hence, we opt for the more conservative result from M. Rosario-Franco et al. (2020) because their results uniformly sample the moon's starting orbital phase as our outwardly migrating moons encounter the chaotic region near the stability domain randomly. The moon's lifetime corresponds to the simulation termination time or the full simulation time (200 Myr).

#### 2.4. Secular Tidal Evolution:

To explore longer evolution timescales of the moon, we utilize a secular tidal evolution (R. Barnes 2017) to compare to our `rebound` results. The following equations detail the semi-major axis, eccentricity, and spin axis evolution of both the moon and planet orbit with all symbols having their usual meaning:

**Table 1.** Initial conditions for `rebound` simulations for M0, M2, and M4 systems.

	$M_*$ ( $M_\odot$ )	$T_*$ (K)	$L_*$ ( $L_\odot$ )	$M_p$ ( $M_\oplus$ )	$a_p$ (au)	$e_p$	$k_2$	$\bar{C}$	$P_s$ (h)	$\tau_p$ (s)	$M_m$ ( $M_\oplus$ )	$a_m$ (au)	$e_m$
M0	0.57	3850	0.0690	0.8–2.0	0.27–0.52	0.03	0.298	0.3308	5	698	0.0123	$3R_{\text{Roche}}$	$10^{-6}$
M2	0.44	3560	0.0290	...	0.17–0.35	...	...	...	...	...	...	...	...
M4	0.23	3210	0.0072	...	0.08–0.18	...	...	...	...	...	...	...	...

NOTE—The quantities  $M_{*/p/m}$  represent the masses of the star, planet, and moon, respectively, while  $a_{p/m}$  and  $e_{p/m}$  denote the semi-major axes and eccentricities of the planet and moon.  $R_{\text{Roche}}$  represents the Roche limit of a fluid satellite. The symbols  $T_*$  and  $L_*$  correspond to the stellar surface temperature and luminosity. The parameter  $k_2$  refers to the Love number of the planet, while  $\bar{C}$ ,  $P_s$ , and  $\tau_p$  represent the moment of inertia constant, the initial spin period, and the time-lag constant for the planet, respectively. Repeated parameters are indicated by ellipses.

$$\frac{da}{dt} = \frac{2a^2}{GM_1M_2} \sum_{i=1}^2 Z_i \left( \cos(\psi_i) \frac{f_2(e)}{\beta^{12}(e)} \frac{\Omega_i}{n} - \frac{f_1(e)}{\beta^{15}(e)} \right) \quad (3)$$

$$\frac{de}{dt} = \frac{11ae}{2GM_1M_2} \sum_{i=1}^2 Z_i \left( \cos(\psi_i) \frac{f_4(e)}{\beta^{10}(e)} \frac{\Omega_i}{n} - \frac{18}{11} \frac{f_3(e)}{\beta^{13}(e)} \right) \quad (4)$$

$$\frac{d\Omega_i}{dt} = \frac{Z_i}{2M_i r_g^2 R_i^2 n} \left( 2 \cos(\psi_i) \frac{f_2(e)}{\beta_{12}(e)} - [1 + \cos^2 \psi_i] \frac{f_5(e)}{\beta^9(e)} \frac{\Omega_i}{n} \right) \quad (5)$$

where

$$Z_i \equiv 3G^2 k_{2,i} M_j^2 (M_i + M_j) \frac{R_i^5}{a^9} \tau_i \quad (6)$$

and

$$\begin{aligned} \beta(e) &= \sqrt{1 - e^2}, \\ f_1(e) &= 1 + \frac{31}{2} e^2 + \frac{255}{8} e^4 + \frac{185}{16} e^6 + \frac{25}{64} e^8, \\ f_2(e) &= 1 + \frac{15}{2} e^2 + \frac{45}{8} e^4 + \frac{15}{16} e^6, \\ f_3(e) &= 1 + \frac{4}{3} e^2 + \frac{8}{9} e^4 + \frac{5}{64} e^6, \\ f_4(e) &= 1 + \frac{3}{2} e^2 + \frac{1}{8} e^4, \\ f_5(e) &= 1 + 3e^2 + \frac{3}{8} e^4. \end{aligned} \quad (7)$$

These calculations explore expected moon lifetimes due to solely tidal effects in contrast with our numerical simulations which additionally account for mean

motion and other non-secular effects. Each simulation evolves up to 5 Gyr utilizing the same termination criterion as in our numerical simulations with `rebound`. From these secular tidal theory calculations, we extend our `rebound` results for initial parameters ( $a_p$ ,  $m_p$ ) that survive for 200 Myr while also investigating how this analytical method compares to our more robust numerical results.

## 2.5. Maximum Lifetimes through Extrapolation

To estimate the maximum lifetimes of these long-lived cases (i.e., those that survive 200 Myr), we use an extrapolation method based on the `rebound` simulation output. After  $\sim$ 10 Myr the tidal migration proceeds quasi-linearly in logarithmic time, which allows us to apply a first-order regression to this late-stage migration. For each case, we randomly select 1,000 intervals with start times between 20–100 Myr and end times at the simulation limit. The moon’s stability limit is fitted (in log time), incorporating both  $e_m$  and  $e_p$  (M. Rosario-Franco et al. 2020), with an additional regression. The intersection of the migration and stability-limit fits defines the estimated time of instability, or maximum lifetime.

We test our method’s predictive power using simulations with lifetimes between 30–100 Myr as an ideal testbed. These cases work perfectly because we already know the final outcome (i.e., the moon’s actual lifetime) and the migration period after 10 Myr is long enough to perform a reliable regression. We then compare our regression-based lifetime estimates against these known outcomes, computing the percent error to quantify any systematic bias in our method.

### 3. RESULTS AND DISCUSSION

#### 3.1. General Comments

Using `rebound` and `reboundx`, we perform N-body simulations with tidal effects to explore exomoon stability in a 3-body system around an M0, M2, and M4 dwarf. The mass  $M_p$  and semi-major axis  $a_p$  of the planet is varied with the  $a_p$  spanning the HZ of the given star. We track exomoon lifetime up to 200 Myr following the moon’s formation, where individual simulations are terminated when the moon crosses the stability limit (M. Rosario-Franco et al. 2020).

By varying the planet’s mass and its semi-major axis, we broadly sample the region where the planet’s gravity dominates because both parameters can modify the planet’s Hill radius. Broadly, our numerical simulations show that moon lifetimes scale with the Hill radius: a larger Hill sphere lengthens the migration path before escape. The host star and the moon tidally interact with the planet to slow down its spin. Since the moon’s orbit initially lies beyond the co-rotation radius, the moon migrates outward. This tidal interaction is modulated by the tidal time-lag  $\tau_p$ , which sets the phase offset between the tidal bulge and the line of centers.

The tidal time-lag of the planet quantifies how efficiently tidal energy is dissipated and the angular momentum transferred to the moon via a torque. Varying  $\tau_p$  reflects how composition and structure shape the tidal response through de-spinning, and the moon’s orbital evolution. The modern Earth has a  $\tau_p$  of 698 seconds, which we adopt in most simulations and represents the tidal strength expected for a world with a significant water ocean. In contrast, we also employ models with weaker tides ( $\tau_p = 100$  and 10 seconds) using secular tidal theory (R. Barnes 2017), which evaluate an expected dry-Earth scenario and an even more extreme (yet unknown) composition, respectively. In the absence of information on the true composition of these worlds, we characterize the dry-Earth as a “weak tide” and the case of  $\tau_p = 10$  s as a “very weak tide”. The tidal dissipation efficiency of a planet can also be expressed via the tidal quality factor,  $Q_p$  (see recent examples from J. Leconte et al. 2010; R. Heller et al. 2011; R. Barnes 2017).

According to T. Sasaki et al. (2012),  $Q_p$  typically ranges from 10–500 for rocky planets and exceeds  $10^4$  for ice and gas giants. Using the  $Q_p$ – $\tau_p$  relation ( $\tau_p \sim 1/Q_p$ ) (J. Leconte et al. 2010; R. Heller et al. 2011), a time-lag of  $\tau_p = 100$  s corresponds to  $Q_p \approx 638$ , near the upper limit for rocky bodies, while  $\tau_p = 10$  s gives  $Q_p \approx 6380$ , approaching values typical of Jovian planets. These cases represent weaker tidal dissipation regimes,

serving as points of comparison to the Earth-like baseline. Secular tidal theory allows us to probe billion-year timescales where N-body simulations are too computationally expensive.

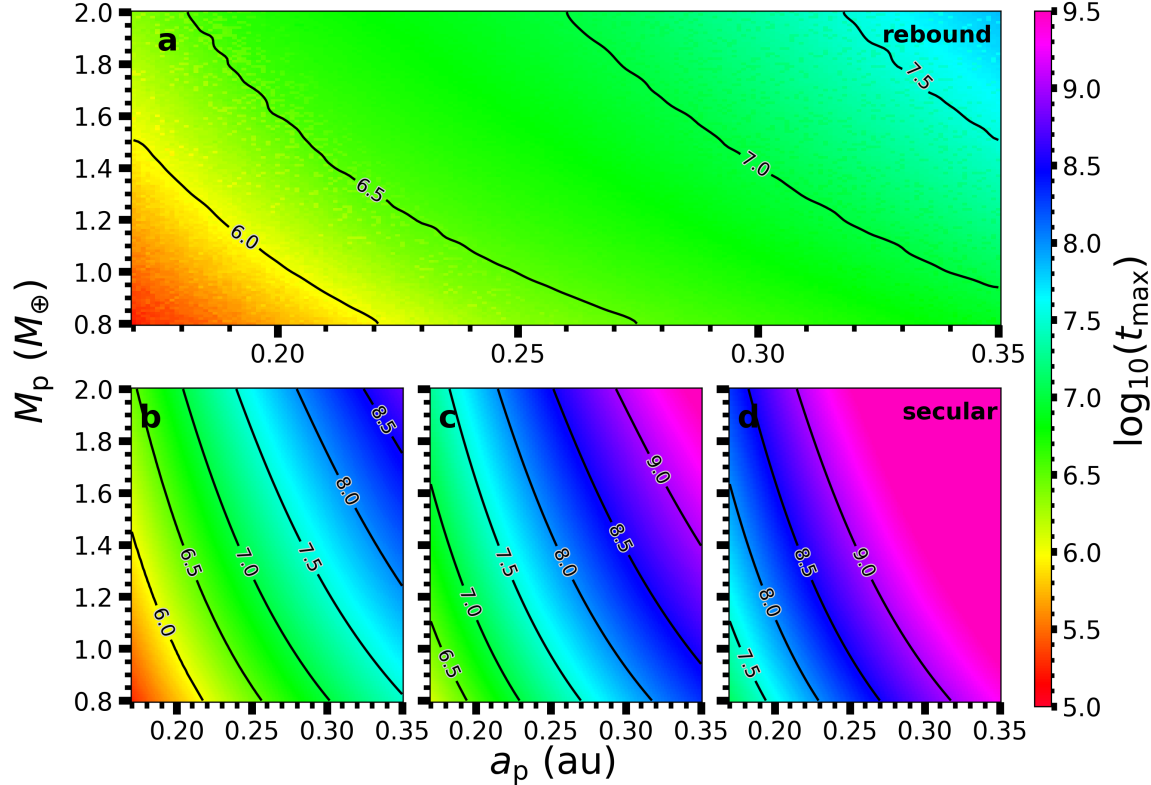
#### 3.2. Habitable Zone Moons in M2-dwarf systems

Figure 2 illustrates the results of our simulations with color-coded cells where the color represents the exomoon’s lifetime depending on the initial condition ( $a_p$ ,  $M_p$ ). With Earth-like tides ( $\tau_p = 698$  s), the `rebound` results (Fig. 2a) differ markedly with those using the tidal secular approximation (Fig. 2b), where moon lifetimes are  $< 100$  Myr for the former and up to  $\sim 100$  Myr for the latter. When the moon resides deep within the planet’s potential well, the secular tidal equations predominantly govern its evolution and the N-body perturbations are minimized. Eventually, mean motion resonances (MMRs) and other three-body effects become significant leading to the observed divergence in evolutionary behavior. Since `rebound` accounts for the increasingly significant perturbations on the mean-motion timescale, its results are considered more physically reliable than those derived from the tidal secular theory, which assumes that these perturbations are always small. If we assume weaker tides ( $\tau_p = 100$  s; Fig. 2c), the moon lifetimes extend to  $\sim 1 - 2$  Gyr. In the very weak regime ( $\tau_p = 10$  s; Fig. 2d), some moons survive nearly 5 Gyr before reaching the stability limit.

From the `rebound` results, we find that the moon migrates to the stability limit between  $\sim 1 - 50$  Myr following a two-phase migration. The first phase of evolution aligns with the secular tidal model while the second phase is triggered as the moon crosses the 15 : 1 MMR. As the moon migrates outward, each resonance crossing takes longer and imparts a stronger kick, amplifying the moon’s eccentricity (Figs. 3a-f). Due to the slower migration, the MMRs force the orbital evolution to deviate from the secular tidal model. In this second phase, the moon spends more time within the MMRs and the kicks from the host star lead to higher  $e_m$  that are not damped by tidal dissipation (Figs. 3g-i).

If we start the planet at the inner edge of the HZ ( $a_p = 0.17$  au; Figs. 3a, 3d, and 3g), the `rebound` evolution generally follows the secular tidal evolution. Due to the faster spin-down of the planet from the star and the quicker overall evolution of the system, the tidal migration overwhelms the 3-body and MMR effects. The moon’s eccentricity still increases because the secular forcing timescale is only  $\sim 10^3 - 10^4$  yr, which is short compared to the migration timescale.

If we instead start the planet at the outer edge of the HZ ( $a_p = 0.34$  au; Figs. 3c, 3f, and 3i), the `rebound`



**Figure 2.** Stability simulation results for a HZ planet–moon orbiting an M2-dwarf. Logarithm of maximum moon lifetime ( $\log_{10}[t_{\max}]$ ) from simulations considering a range of host planet masses (0.8 to  $2 M_{\oplus}$ ) and semi-major axis within the HZ of an M2-dwarf. (a) shows results from N-body simulations using `rebound` with a tidal time-lag  $\tau_p$  of 698 s, while (b-d) show outcomes from secular tidal theory (R. Barnes 2017) with tidal dissipation timescales  $\tau_p$  of (b) 698 s, (c) 100 s, and (d) 10 s. Contour lines indicate  $\log_{10}(t_{\max})$  values, reflecting the time of moon loss due to tidal migration. Red, yellow, green, and blue regions represent increasingly longer lifetimes while purple regions represent the longest lifetimes.

simulations only follow the secular tidal evolution up to  $\sim 5 - 8$  Myr, after which the second phase in the evolution occurs due to MMR exposure and the rebound simulations deviate from the secular calculations. After the bump in the  $a_m$  evolution, the migration rate slows and follows the secular evolution. In this later evolution stage, the moon encounters fewer MMRs as the gap between MMRs widens at lower values of N:1. In addition to the eccentricity pumping, the moon’s semi-major axis  $a_m$  oscillates (see Fig. 3b and Fig. 3c) at later times, indicative of strong interactions with the MMRs or strong kicks directly from the host star.

A typical bump in the moon’s semi-major axis is  $\sim 0.035$  to  $\sim 0.050 R_H$  due to the MMRs and other effects. We apply this bump to the secular tidal evolution to mimic these extra effects on top of our secular results, where for the M2 case with very weak tides ( $\tau_p = 10$  s, Fig. 2d), only a few parameters remain marginally stable. It is important to note that a  $\tau_p$  of 10 seconds may require an exotic (maybe nonphysical) interior for the planet considered here and is therefore unlikely.

The moon’s outward migration is fueled by the angular momentum transfer, where the planet’s rotational period after  $\sim 10$  Myr increases only up to  $\sim 7 - 11$  hr (Fig. 4) in the `rebound` simulations. Previous studies (J. W. Barnes & D. P. O’Brien 2002; T. Sasaki et al. 2012; A. L. Piro 2018) using the constant  $Q$  model for tides showed that moons can escape planets even if they start with more slowly rotating planets. Our simulations use a stability limit prescription (i.e., M. Rosario-Franco et al. 2020) that excludes the chaotic transition region that is phase-dependent, but if we consider larger stability limit up to  $\sim 0.5 R_H$  (i.e., R. C. Domingos et al. 2006), the outward migration will continue until this threshold is crossed ( $\sim 100$  Myr).

### 3.3. Habitable Zone Moons in M4-dwarf systems

For the case of an M4-dwarf, the HZ is closer-in and narrower, where we see a similar gradient in moon lifetimes with the planetary mass and initial semi-major axis. Figure 5 shows our M4 results, but with a distinct cubehelix colormap (compared to the rainbow colormap in Fig. 2) to emphasize the differing colorbar

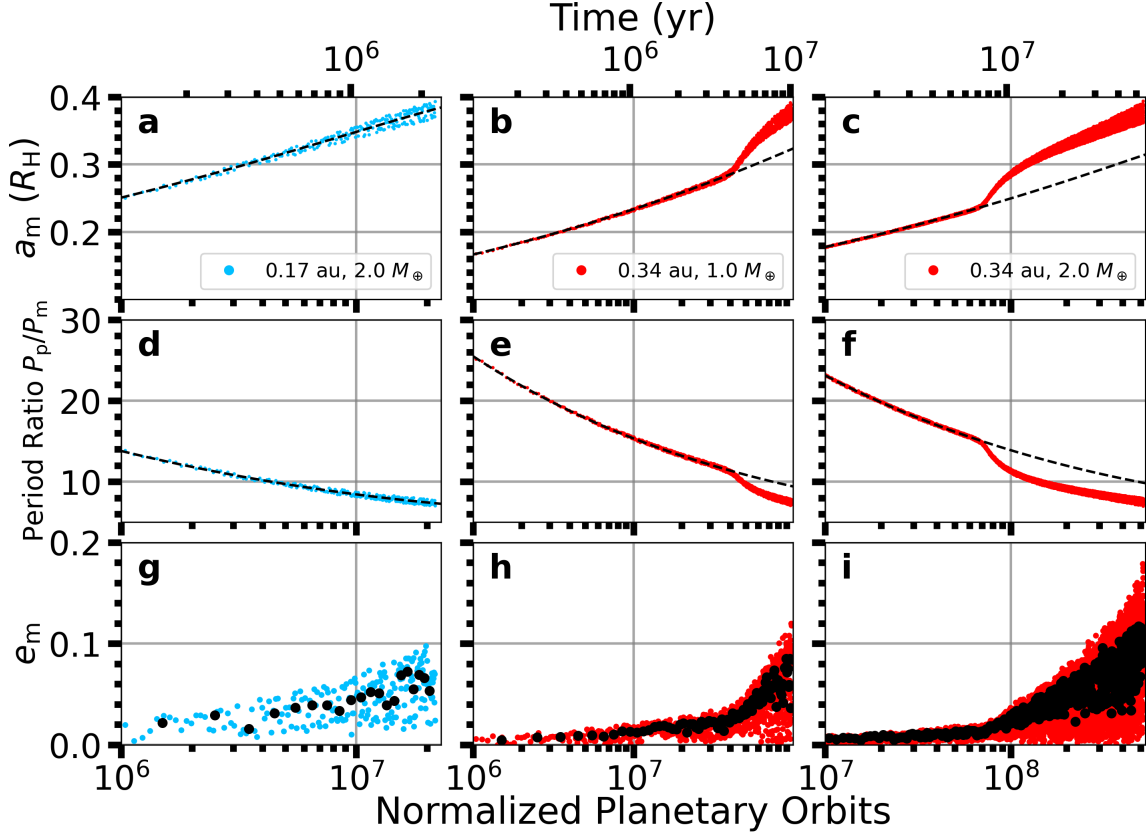


**Figure 3.** Time evolution for three HZ planet–moon systems orbiting an M2-dwarf. Time evolution of the (a-c) exomoon’s semi-major axis  $a_m$ , (d-f) planet to moon period ratio  $P_p/P_m$ , and (g-i) exomoon’s eccentricity  $e_m$  for 3 distinctive points in the parameter space (0.17 au and  $2.0 M_{\oplus}$ , 0.34 au and  $1.0 M_{\oplus}$ , 0.34 au and  $2.0 M_{\oplus}$ ) in the M2 case. The bottom  $x$ -axis, plotted on a logarithmic scale, shows time normalized by the orbital period of a planet at the inner edge of the HZ (0.17 au) while the top  $x$ -axis shows time (in years). The blue and red points signify rebound results while black dashed lines represent results from secular tidal theory. Black dots in the eccentricity panels represent the median value over 1 million orbits.

limits. Notably, all the simulations in this parameter space terminate before 10 million years (Fig. 5). Since the HZ around an M4-dwarf is closer-in, the tidal effects from the host star are much stronger and the moon’s migration is faster, allowing it to escape on a shorter timescale. Additionally, we expect potential moons orbiting Earth-like planets within the HZs of later (M4+) dwarfs to showcase a similar behavior (S. R. Kane 2017). By contrast, the HZs of earlier M-dwarfs the HZ extends farther out, which weakens tidal effects from the host star and opens the possibility of longer-lived moons.

#### 3.4. Habitable Zone Moons in M0-dwarf systems

For an M0-dwarf, the HZ extends farther out and spans a wider range because of the star’s higher luminosity. This geometry shifts the balance, where moons can survive much longer before reaching instability. As a result, there is a shift towards longer lifetimes due to the longer orbital periods and the overall weaker stellar tide at larger distances (Fig. 6). We model systems with Earth-like tides ( $\tau_p = 698$  s) up to 200 Myr to

capture the outward migration from  $\sim 8 - 60 R_p$ . The stability limit for the outer HZ in these systems is  $\sim 66 R_p$  (M. Rosario-Franco et al. 2020), where those simulations that survive for 200 Myr are shown by the upper right region beyond the white contour (Fig. 6a).

Beyond the white contour, we use polynomial fits to extrapolate and estimate the lifetimes of these cases. Similar to our results for an M2-dwarf (see §3.2, a bump in migration rate due to MMRs appears just before  $\sim 10$  Myr (see Fig. 7). We therefore apply a best-fit line (using `numpy.polyfit`; C. R. Harris et al. (2020)) to the later stages of the moon’s evolution, when tidal migration proceeds quasi-linearly in logarithmic time. To reduce bias from the starting point, we perform 1,000 fits with intervals beginning at  $\sim 20 - 100$  Myr and extending to 200 Myr.

In addition, we account for changes in the moon’s eccentricity over the same interval and its effect on the computed stability limit (M. Rosario-Franco et al. 2020), incorporating the effects of both moon and planetary

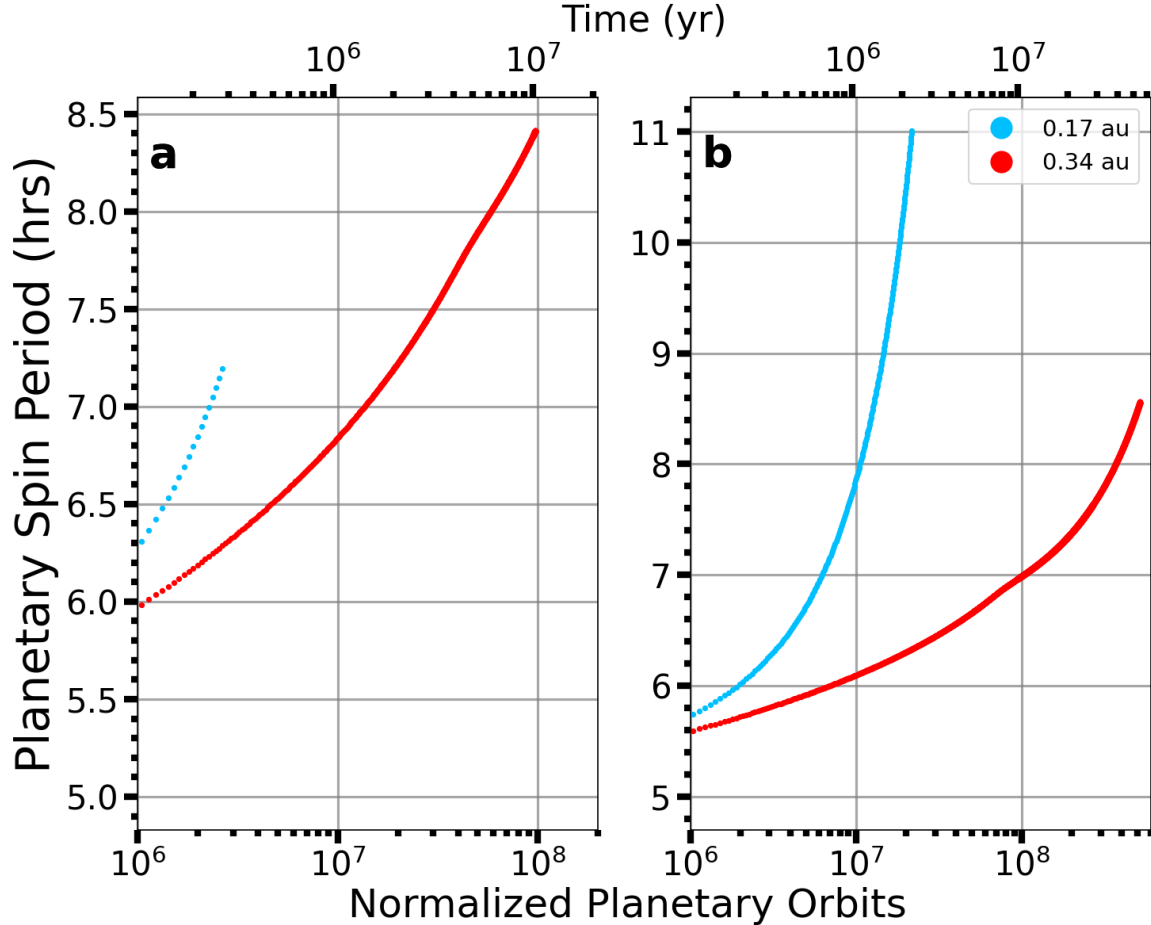


**Figure 4.** Spin evolution for four HZ planet–moon systems orbiting an M2-dwarf. Evolution of planetary spin period for two  $a_p$  cases in the M2 parameter space (0.17 au, 0.34 au) at (a)  $1.0 M_{\oplus}$  and (b)  $2.0 M_{\oplus}$  from `rebound` simulations where curve lengths represent lifetimes. The bottom  $x$ -axis, plotted on a logarithmic scale, shows time normalized by the orbital period of a planet at the inner edge of the HZ (0.17 au) while the top  $x$ -axis shows time (in years).

eccentricities ( $e_m$  and  $e_p$ ). The intersection point of the best-fit line for the moon’s extrapolated semi-major axis and the stability limit estimates the time when the moon reaches the stability threshold (Fig. 8). Each of the 1,000 fits has a slightly different slope, which results in a range in the projected lifetime. The longest-lived system lies at the upper right of the  $M_p - a_p$  parameter space (i.e., 0.52 AU,  $2 M_{\oplus}$ ), where we find a mean lifetime of  $\sim 1.61$  Gyr with a  $1\sigma$  confidence interval of roughly 1.52–1.70 Gyr.

When second-order polynomial fits are applied, the estimated mean lifetime decreases to  $\approx 1.16$  Gyr, with a corresponding  $1\sigma$  range of  $\approx 1.05$ –1.26 Gyr. Higher-order polynomial fits are possible but lack physical plausibility because they can have a negative curvature. We therefore adopt the first-order fits, which provide the most optimistic lifetime and physically interpretable results. To assess the robustness of these best-fit calculations, we repeat the analysis for the region below the

white curve, focusing specifically on cases with lifetimes in the 30–100 Myr range and compare the estimated lifetimes to actual values obtained from simulations.

On average, the best-fit approach yields a lifetime estimate that is approximately 16% longer than the simulated values, with a  $1\sigma$  range of 9.3% to 23.6%. As the eccentricity grows (see Figs. 7g–i), the semi-major axis evolution can accelerate toward the end of the moon’s lifetime, resulting in a migration rate faster than the simple best-fit model. If we correct for this bias in our original results, the revised longest-lived estimate is  $\approx 1.35$  Gyr.

We further probe the outward migration of the moon by exploring the time series evolution for a few points in the M0 parameter space in a similar manner as in Sec. 3.2. If we consider a moon-hosting planet at the inner edge of the HZ (0.27 au,  $2.0 M_{\oplus}$ ; Fig. 7a), we see a relatively smooth evolution of  $a_m$  until around 5 Myr where the planet–moon period ratio reaches about 10:1 and

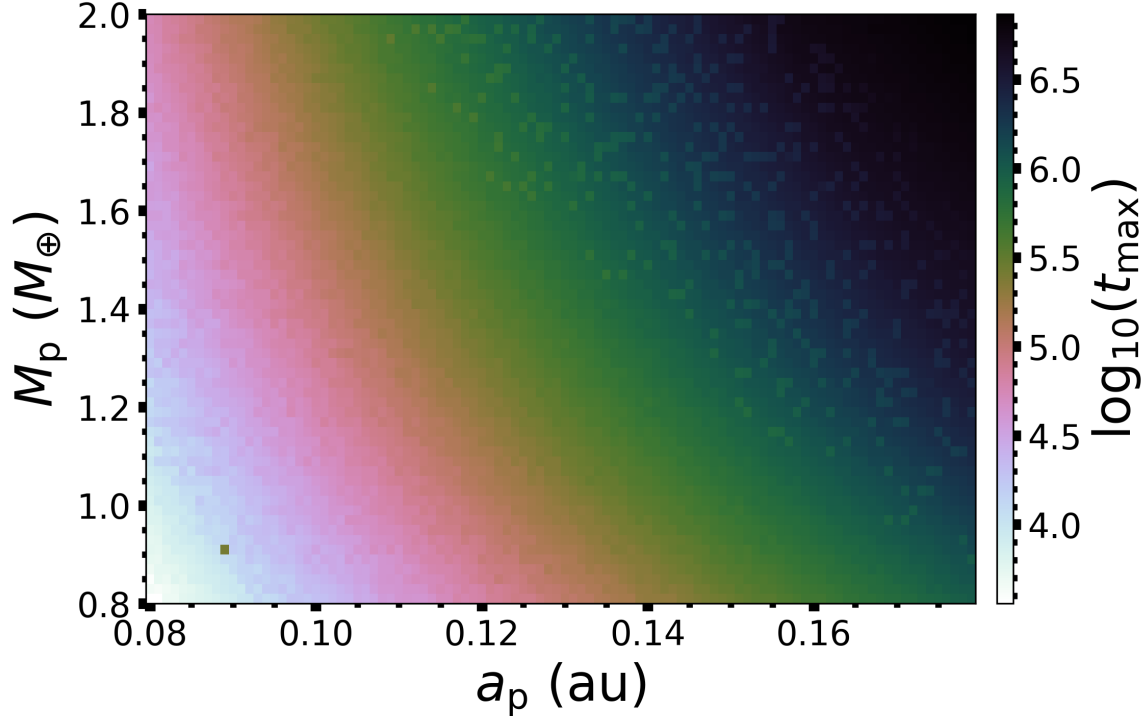


**Figure 5.** Stability simulation results for a HZ planet–moon orbiting an M4-dwarf. Logarithm of maximum moon lifetime ( $\log_{10}[t_{\max}]$ ) from `rebound` simulations for considering a range of host planet masses (0.8 to  $2 M_{\oplus}$ ) and semi-major axis within the HZ of an M4-dwarf.

MMRs induce a bump in the migration rate (Fig. 7d). If we instead consider Earth-like planets ( $1 M_{\oplus}$  or  $2 M_{\oplus}$ ) orbiting at the outer edge of the HZ (0.52 au), the evolution of  $a_m$  (Figs. 7b and 7c) also has a noticeable bump due to the exposure to MMRs; however, the boost in migration is not enough to bring the moon to the stability limit in the time allowed for the more massive ( $2 M_{\oplus}$ ) case. We note that this bump is also on the order of  $0.035 R_{\text{H}}$  where the evolution of the moon then stabilizes to a similar slope to the secular theory afterwards.

From a secular tide model assuming Earth-like tides, we find the vast majority of the initial conditions are unstable within 5 Gyr, barring the top right portion (Fig. 6b). When adding the bump of  $0.035 R_{\text{H}}$ , we find these survivors should migrate past the stability limit to eventually become unstable. In the weak tide limit ( $\tau_p = 100$  s; Fig. 6c), the top right region with billion-year lifetimes grows larger and after adding the bump, we find that only a small region of the  $M_p$ – $a_p$  parameter space remains within the stability limit. For the very weak tide case ( $\tau_p = 10$  s; Fig. 6d), the majority of lifetimes are billions of years. Such a small tidal lag implies an unusual planetary interior, requiring further study to assess plausibility.

We examine the secular tidal migration considering a  $2.0 M_{\oplus}$  planet orbiting at the outer edge of the HZ (0.52

au) because it has the slowest evolution (Fig. 9), where it takes 1 Gyr for the moon to reach  $\sim 0.33 R_{\text{H}}$ . By incorporating the bump in the migration rate into our secular results, the moon will migrate to  $\sim 0.365 R_{\text{H}}$  within 1 Gyr, which closely approaches the stability threshold (Fig. 9a) and crosses the stability limit by 1.3 Gyr. This lifetime estimate is comparable to the estimate from our extrapolation method, further reinforcing the system’s susceptibility to instability.

#### 4. SUMMARY AND CONCLUSIONS

Our findings suggest that HZ Earth-like planets in M-dwarf systems will lose large (Luna-like) moon(s) (if formed) within the first billion years of their existence. The planetary HZs vary depending on the spectral subtype of the host star, which in turn varies the strength of the stellar tides. Our 200 Myr numerical simulations of star–planet–moon systems orbiting the HZ of M4-dwarfs show the typical moon lifetime is less than 10 Myr (Fig. 5), which is very short compared to the astrobiological, geological, or astrophysical timescales. Given these outcomes, we expect similar systems orbiting in the HZs of later M-dwarfs (M5–M9) to lose their moon(s) on even shorter timescales (S. R. Kane 2017).

These results echo earlier work on giant-planet moons in M-dwarf systems. Using tidal and dynamical models, R. R. Zollinger et al. (2017) showed that massive exo-

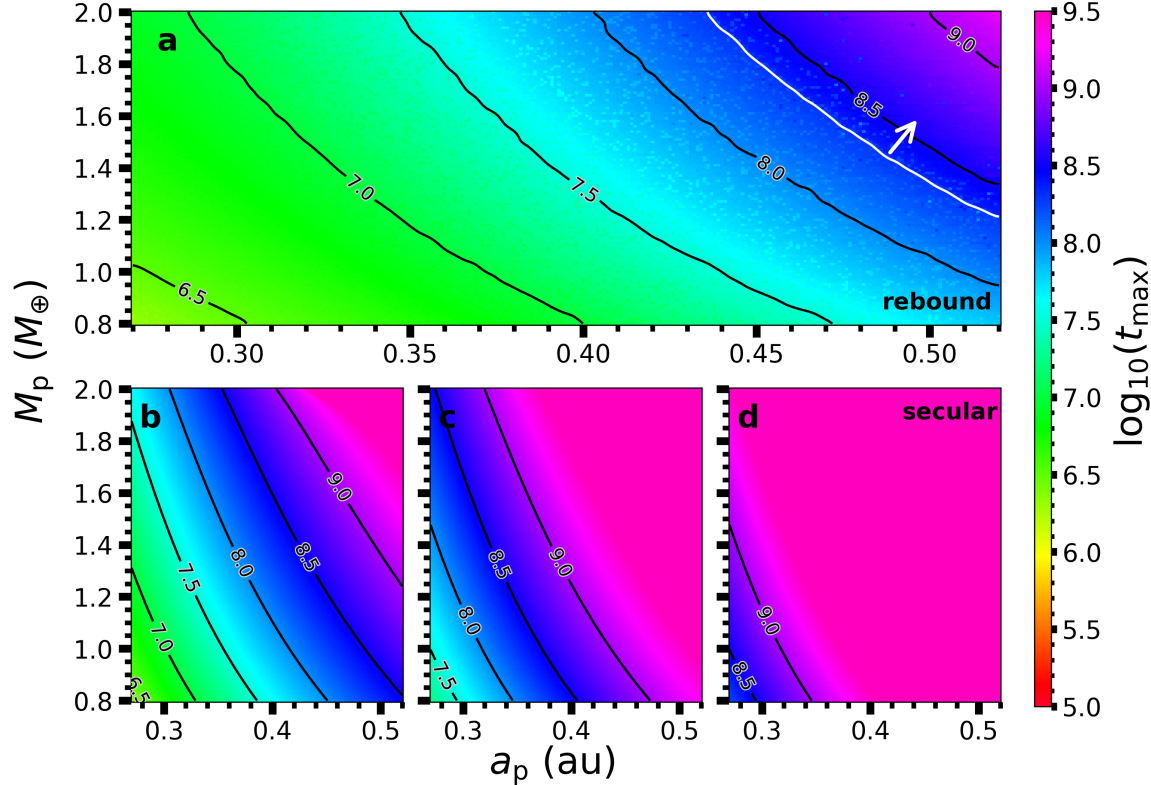


**Figure 6.** Stability simulation results for a HZ planet–moon orbiting an M0-dwarf. Similar to Fig. 2 but for moons orbiting an Earth-sized planet in an M0 system. The white contour in (a) marks the boundary beyond which the lifetimes are extrapolated, as indicated by the arrow. The maximum lifetime in (a) is  $\approx 9.2$  in  $\log_{10}(t)$ .

moons are unlikely to sustain habitable conditions due to extreme tidal heating, and that moons orbiting lower-mass M-dwarfs are dynamically unstable. Together with our findings, this points to a general fragility of exomoons in M-dwarf systems. An early M2-dwarf system does not provide a haven for moon(s) either, where such a moon can survive a while longer. The moon’s outward migration will cross the stability limit (M. Rosario-Franco et al. 2020) within 1–50 Myr. The broad range of moon lifetimes depends on the planet’s placement within the HZ and the assumed composition through the tidal time-lag.

A large moon’s lifetime can reach 1 Gyr if it orbits a habitable Earth-mass planet orbiting an M0-dwarf. This configuration is special because its outer HZ edge extends to 0.52 au, which weakens the stellar tide on the host planet and leaves a large part of the tidal action to the moon’s tide that despins the host planet. When considering an Earth-like tidal time-lag ( $\tau_p = 698$  s; possibly an ocean-world Earth) and a more massive host planet ( $M_p = 2 M_\oplus$ ), we find a maximum moon lifetime of 1.35 Gyr. This timescale corresponds to a time on the Earth when oxygen was just beginning to buildup in our atmosphere.

Even longer lifetimes ( $>5$  Gyr) may be possible, but these require lower-mass moons or an exotic host planet composition so that the tide is less effective ( $\tau_p \lesssim 100$ ; a dry-Earth or weak tide). Higher-mass planets located in the outer regions of the HZs within M0-type stellar systems may be the only configuration to host large, observable (and potentially habitable (H. Martínez-Rodríguez et al. 2019)) moons. Smaller, low-mass moons (e.g., Phobos / Ceres-like) would still be possible; however, if present, they would exist beyond the current limits of photometric detectability (relative to the noise floor) or reveal themselves through transit-timing variations (D. M. Kipping 2009). If a moon is indeed required for complex life to develop on a host planet, our results suggest that this limitation may represent an additional contributing factor to the Drake equation and Fermi paradox, as M-dwarfs dominate the stellar population yet appear largely unable to host large, HZ moons.

It is important to note that M0–M4 dwarfs have pre-main-sequence lifetimes of  $\approx 200$ –400 Myr (R. M. Ramirez & L. Kaltenegger 2014). Throughout this phase, planets orbiting these stars are subjected to intense flaring activity and elevated UV flux, conditions that may inhibit or delay the emergence of life (R. Luger

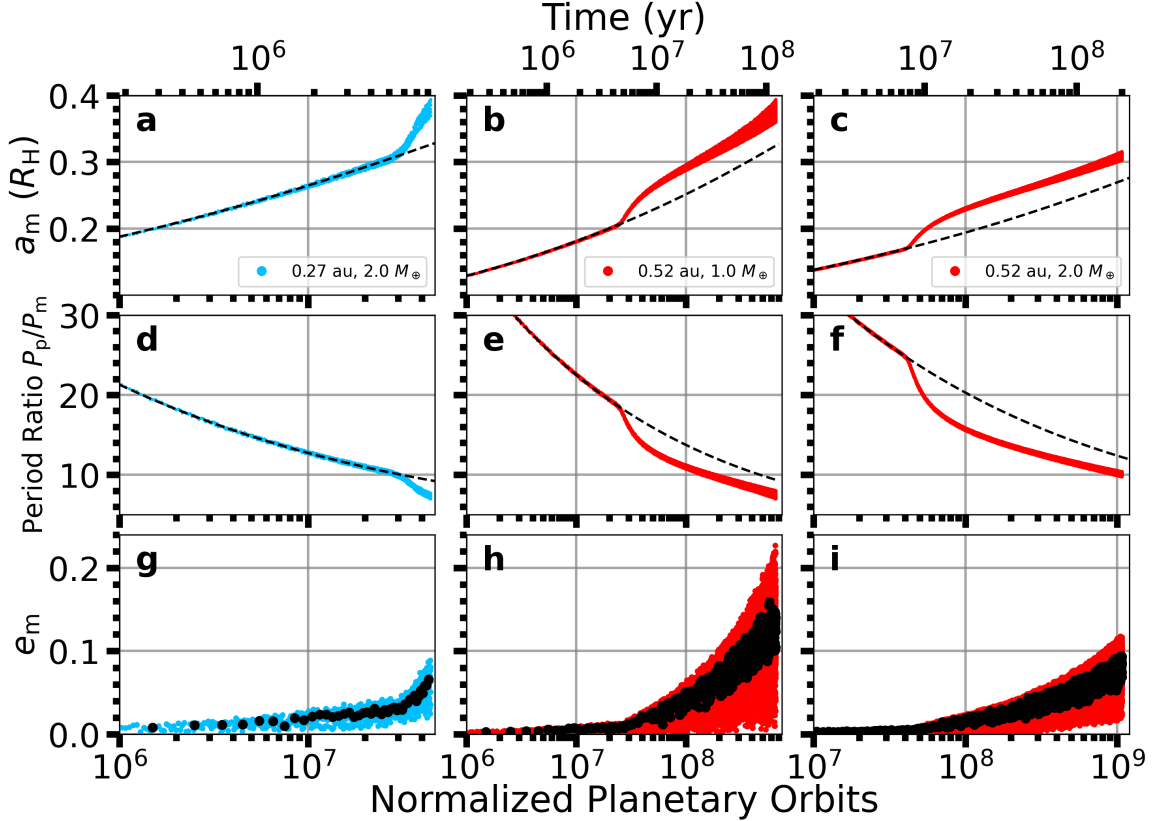


**Figure 7.** Time series plot for three HZ planet–moon systems orbiting an M0-dwarf. Same as Fig. 3 but for moons in an M0 system. The 3 distinct points used are (0.27 au and  $2.0 M_{\oplus}$ , 0.52 au and  $1.0 M_{\oplus}$ , 0.52 au and  $2.0 M_{\oplus}$ ). The bottom  $x$ -axis uses 0.27 au as the inner edge of the HZ for normalization.

& R. Barnes 2015; K. V. Getman et al. 2022). Under such circumstances, large moons orbiting these planets would likely already have become dynamically unstable prior to the emergence of life in this delayed timeline.

Additionally, when considering planetary occurrence rates around M-dwarfs, we expect on average one to two Earth-sized planets per star, with a bias toward short-period systems (E. Gaidos et al. 2016; K. K. Hardegree-Ullman et al. 2019). For HZ planets, C. D. Dressing & D. Charbonneau (2015) estimate an occurrence rate of 0.24 Earth-sized planets per M-dwarf, while D. C. Hsu et al. (2020) report a rate of 0.33 for planets with radii between  $0.75$  and  $1.0 R_{\oplus}$ . As future surveys shift focus toward longer-period HZ planets, Earth-like planets orbiting within the HZs of M-dwarfs are expected to be a central part of future observational campaigns.

## 5. OUTLOOK

The Habitable Worlds Observatory (HWO), a proposed 6 – 8 meter space telescope, is a promising tool in the search for exomoons, in addition to its main task of finding habitable Earth-like exoplanets (E. National Academies of Sciences 2021). With this telescope the detection of Luna-sized exomoons may be possible (M. A.

Limbach et al. 2024). Given our results, such a telescope might (1) detect HZ moons orbiting Earth-like planets around M0-dwarfs (depending on the system’s age) and (2) provide observational verification (according to the instrumental detection limit) for the absence of HZ exomoons around those planets in systems with host stars of spectral type M2 or later. This mission is built on the concepts of two other proposed space telescopes, LUVOIR (T. LUVOIR Team 2019) and HabEx (B. S. Gaudi et al. 2020).

Moreover, the Giant Magellan Telescope (GMT), a 25.4 meter ground-based observatory currently under construction will offer improved spatial resolution and sensitivity, allowing for the direct imaging of exoplanets and the possible detection of exomoons through methods such as direct imaging (R. A. Bernstein et al. 2014). In addition to established methods used in exoplanet detection such as photometry and transit timings (A. Teachey 2024), emerging observational techniques may also prove useful in the detection of exomoons. A. Vanderburg et al. (2018) provides novel radial velocity (RV) methods combined with direct imaging while cyclotron

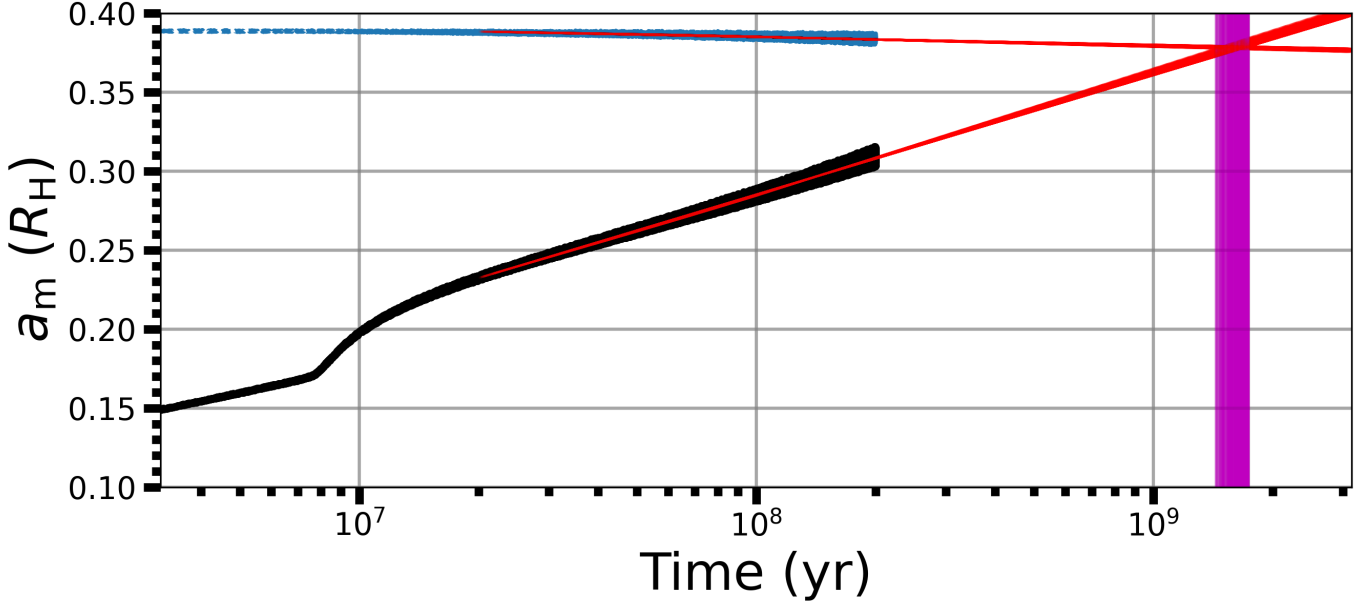


**Figure 8.** Best-fit analysis for the lifetime of one HZ planet–moon system orbiting an M0-dwarf. Time evolution of the exomoon’s semi-major axis for a representative case within the M0 parameter space (0.52 au,  $2.0 M_{\oplus}$ ), computed using `rebound`. Black points denote the `rebound` simulation results, while the blue dashed line indicates the moon’s stability limit. Red curves correspond to best-fit lines for both the stability threshold and the `rebound` evolution. Their intersection, marking the estimated instability time, is highlighted in magenta.

radio emission methods [J. P. Noyola et al. \(2014, 2016\)](#) could emerge useful in exomoon observations.

Two programs were selected for observation in JWST cycle 3 including a search around: (1) a long-period Jupiter-like planet orbiting a K-dwarf ([B. Casse et al. 2024, GO 6491](#)) and (2) a terrestrial HZ planet orbiting an M-dwarf ([E. Pass et al. 2024, GO 6193](#)), which provide two different avenues of exploration. Our work suggests that program (2) would not be successful given the estimated age of TOI-700 is  $> 1.5$  Gyr, the host star is a spectral type M2V, and the host planet (TOI-700d) lies at 0.16 au ([E. A. Gilbert et al. 2020](#)). Even within the very weak tide scenario, the expected moon lifetime is  $\lesssim 100$  Myr (see Fig. 2). Program (1) will attempt to detect Galilean sized moons, which has its own challenges (see [S. C. Millholland & J. N. Winn 2025](#)), but escape via tides is of no concern.

## ACKNOWLEDGMENTS

The authors thank the anonymous reviewer whose comments greatly improved the quality of the manuscript. S.D.P. and N.N.W. acknowledge support by the National Science Foundation (NSF) under grant No. AST-2054353. B.Q. acknowledges support in part by the Texas A&M High Performance Research Computing (HPRC) and the NSF under grant No. 2232895. The authors acknowledge the Texas A&M HPRC for providing computing resources on the Launch cluster that contributed to the research results reported here.

*Software:* `rebound` ([H. Rein & S. F. Liu 2012](#)), `reboundx` ([D. Tamayo et al. 2020](#))

## REFERENCES

Barnes, J. W., & O’Brien, D. P. 2002, *ApJ*, 575, 1087, doi: [10.1086/341477](https://doi.org/10.1086/341477)

Barnes, R. 2017, *Celestial Mechanics and Dynamical Astronomy*, 129, 509, doi: [10.1007/s10569-017-9783-7](https://doi.org/10.1007/s10569-017-9783-7)

Bernstein, R. A., McCarthy, P. J., Raybould, K., et al. 2014, in *Society of Photo-Optical Instrumentation Engineers (SPIE) Conference Series*, Vol. 9145, *Ground-based and Airborne Telescopes V*, ed. L. M. Stepp, R. Gilmozzi, & H. J. Hall, 91451C, doi: [10.1117/12.2055282](https://doi.org/10.1117/12.2055282)

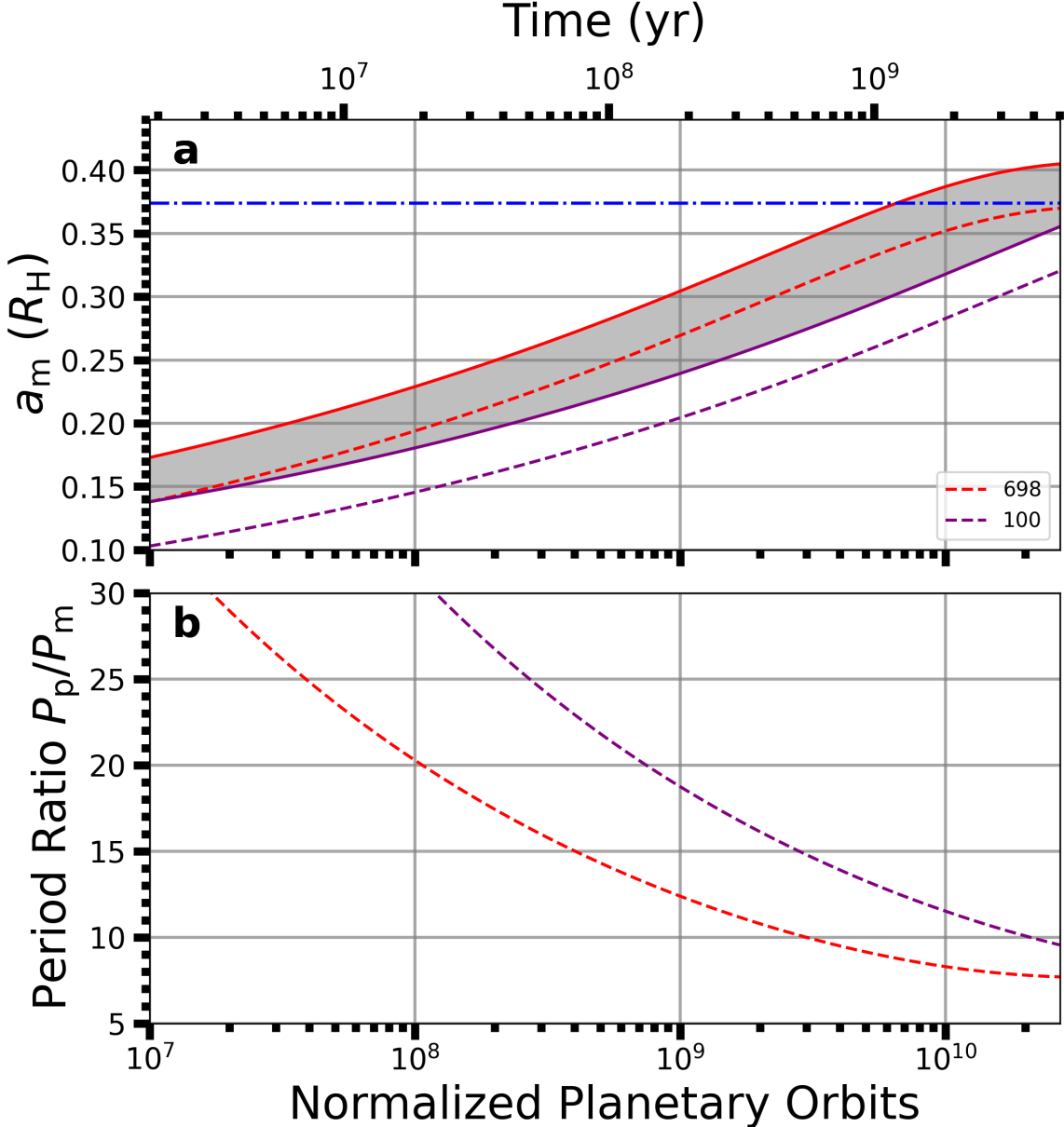


**Figure 9.** Secular evolution of one HZ planet-moon system orbiting an M0-dwarf. Time evolution of the (a) exomoon's semi-major axis  $a_m$  and (b) planet to moon period ratio  $P_p/P_m$  for one case in the M0 parameter space (0.52 au,  $2.0 M_{\oplus}$ ) using secular tidal theory. The bottom  $x$ -axis, plotted on a logarithmic scale, shows time normalized by the orbital period of a planet at the inner edge of the HZ (0.27 au) while the top  $x$ -axis shows time (in years). The red and purple dashed lines represent a  $\tau_p$  of 698 and 100 seconds, respectively, while the red and purple solid lines represent those curves with the added bump of  $0.035 R_H$ , accounting for expected MMR and 3-body effects. The gray shaded region represents the area of expected curves between the boosted 698 second upper limit and boosted 100 second lower limit while the blue dash-dot line represents the moon's stability limit.

Bolmont, Emeline, Raymond, Sean N., Leconte, Jeremy, Hersant, Franck, & Correia, Alexandre C. M. 2015, A&A, 583, A116, doi: [10.1051/0004-6361/201525909](https://doi.org/10.1051/0004-6361/201525909)

Burchell, M. J. 2006, International Journal of Astrobiology, 5, 243, doi: [10.1017/S1473550406003107](https://doi.org/10.1017/S1473550406003107)

Canup, R. M. 2004, ARA&A, 42, 441, doi: [10.1146/annurev.astro.41.082201.113457](https://doi.org/10.1146/annurev.astro.41.082201.113457)

Cassese, B., Batygin, K., Chachan, Y., et al. 2024, Revealing the Oblateness and Satellite System of an Extrasolar Jupiter Analog,, JWST Proposal. Cycle 3, ID. #6491

Chabrier, G. 2003, PASP, 115, 763, doi: [10.1086/376392](https://doi.org/10.1086/376392)

Civiletti, M. 2025, arXiv e-prints, arXiv:2505.00062, doi: [10.48550/arXiv.2505.00062](https://doi.org/10.48550/arXiv.2505.00062)

Cuntz, M., Quarles, B., Eberle, J., & Shukayr, A. 2013, PASA, 30, e033, doi: [10.1017/pas.2013.011](https://doi.org/10.1017/pas.2013.011)

Domingos, R. C., Winter, O. C., & Yokoyama, T. 2006, MNRAS, 373, 1227, doi: [10.1111/j.1365-2966.2006.11104.x](https://doi.org/10.1111/j.1365-2966.2006.11104.x)

Drake, F., & Sobel, D. 1993, Is Anyone Out There?: The Scientific Search for Extraterrestrial Intelligence (Souvenir P.).  
<https://books.google.com/books?id=ZrddHY0mQpgC>

Dressing, C. D., & Charbonneau, D. 2015, ApJ, 807, 45, doi: [10.1088/0004-637X/807/1/45](https://doi.org/10.1088/0004-637X/807/1/45)

Eggleton, P. P., Kiseleva, L. G., & Hut, P. 1998, ApJ, 499, 853, doi: [10.1086/305670](https://doi.org/10.1086/305670)

Gaidos, E., Mann, A. W., Kraus, A. L., & Ireland, M. 2016, MNRAS, 457, 2877, doi: [10.1093/mnras/stw097](https://doi.org/10.1093/mnras/stw097)

Gaudi, B. S., Seager, S., Mennesson, B., et al. 2020, The Habitable Exoplanet Observatory (HabEx) Mission concept study final report,  
<https://arxiv.org/abs/2001.06683>

Getman, K. V., Feigelson, E. D., Garmire, G. P., et al. 2022, ApJ, 935, 43, doi: [10.3847/1538-4357/ac7c69](https://doi.org/10.3847/1538-4357/ac7c69)

Gilbert, E. A., Barclay, T., Schlieder, J. E., et al. 2020, AJ, 160, 116, doi: [10.3847/1538-3881/aba4b2](https://doi.org/10.3847/1538-3881/aba4b2)

Gilbert, E. A., Vanderburg, A., Rodriguez, J. E., et al. 2023, ApJL, 944, L35, doi: [10.3847/2041-8213/acb599](https://doi.org/10.3847/2041-8213/acb599)

Hardegree-Ullman, K. K., Cushing, M. C., Muirhead, P. S., & Christiansen, J. L. 2019, AJ, 158, 75, doi: [10.3847/1538-3881/ab21d2](https://doi.org/10.3847/1538-3881/ab21d2)

Harris, C. R., Millman, K. J., van der Walt, S. J., et al. 2020, Nature, 585, 357, doi: [10.1038/s41586-020-2649-2](https://doi.org/10.1038/s41586-020-2649-2)

Heller, R., Leconte, J., & Barnes, R. 2011, A&A, 528, A27, doi: [10.1051/0004-6361/201015809](https://doi.org/10.1051/0004-6361/201015809)

Heller, R., Williams, D., Kipping, D., et al. 2014, Astrobiology, 14, 798, doi: [10.1089/ast.2014.1147](https://doi.org/10.1089/ast.2014.1147)

Hsu, D. C., Ford, E. B., & Terrien, R. 2020, MNRAS, 498, 2249, doi: [10.1093/mnras/staa2391](https://doi.org/10.1093/mnras/staa2391)

Jagtap, O., Quarles, B., & Cuntz, M. 2021, PASA, 38, e059, doi: [10.1017/pasa.2021.52](https://doi.org/10.1017/pasa.2021.52)

Kaltenegger, L. 2017, ARA&A, 55, 433, doi: [10.1146/annurev-astro-082214-122238](https://doi.org/10.1146/annurev-astro-082214-122238)

Kane, S. R. 2017, ApJL, 839, L19, doi: [10.3847/2041-8213/aa6bf2](https://doi.org/10.3847/2041-8213/aa6bf2)

Kasting, J. F., Kopparapu, R., Ramirez, R. M., & Harman, C. E. 2014, Proceedings of the National Academy of Science, 111, 12641, doi: [10.1073/pnas.1309107110](https://doi.org/10.1073/pnas.1309107110)

Kasting, J. F., Whitmire, D. P., & Reynolds, R. T. 1993, Icarus, 101, 108, doi: [10.1006/icar.1993.1010](https://doi.org/10.1006/icar.1993.1010)

Kipping, D. 2021, Research Notes of the American Astronomical Society, 5, 44, doi: [10.3847/2515-5172/abeb7b](https://doi.org/10.3847/2515-5172/abeb7b)

Kipping, D., & Lewis, G. 2025, International Journal of Astrobiology, 24, e5, doi: [10.1017/S1473550424000235](https://doi.org/10.1017/S1473550424000235)

Kipping, D., Bryson, S., Burke, C., et al. 2022, Nature Astronomy, 6, 367, doi: [10.1038/s41550-021-01539-1](https://doi.org/10.1038/s41550-021-01539-1)

Kipping, D., Teachey, A., Yahalom, D. A., et al. 2025, Nature Astronomy, 9, 795, doi: [10.1038/s41550-025-02547-1](https://doi.org/10.1038/s41550-025-02547-1)

Kipping, D. M. 2009, MNRAS, 392, 181, doi: [10.1111/j.1365-2966.2008.13999.x](https://doi.org/10.1111/j.1365-2966.2008.13999.x)

Kipping, D. M., Forgan, D., Hartman, J., et al. 2013, ApJ, 777, 134, doi: [10.1088/0004-637X/777/2/134](https://doi.org/10.1088/0004-637X/777/2/134)

Kipping, D. M., Nesvorný, D., Buchhabe, L. A., et al. 2014, ApJ, 784, 28, doi: [10.1088/0004-637X/784/1/28](https://doi.org/10.1088/0004-637X/784/1/28)

Kokubo, E., & Genda, H. 2010, ApJL, 714, L21, doi: [10.1088/2041-8205/714/1/L21](https://doi.org/10.1088/2041-8205/714/1/L21)

Kopparapu, R. K., Ramirez, R. M., SchottelKotte, J., et al. 2014, ApJL, 787, L29, doi: [10.1088/2041-8205/787/2/L29](https://doi.org/10.1088/2041-8205/787/2/L29)

Kopparapu, R. K., Ramirez, R., Kasting, J. F., et al. 2013, ApJ, 765, 131, doi: [10.1088/0004-637X/765/2/131](https://doi.org/10.1088/0004-637X/765/2/131)

Kroupa, P. 2001, MNRAS, 322, 231, doi: [10.1046/j.1365-8711.2001.04022.x](https://doi.org/10.1046/j.1365-8711.2001.04022.x)

Kroupa, P. 2002, Science, 295, 82, doi: [10.1126/science.1067524](https://doi.org/10.1126/science.1067524)

Leconte, J., Chabrier, G., Baraffe, I., & Levrard, B. 2010, A&A, 516, A64, doi: [10.1051/0004-6361/201014337](https://doi.org/10.1051/0004-6361/201014337)

Limbach, M. A., Lustig-Yaeger, J., Vanderburg, A., et al. 2024, AJ, 168, 57, doi: [10.3847/1538-3881/ad4a75](https://doi.org/10.3847/1538-3881/ad4a75)

Lu, T., Hernandez, D. M., & Rein, H. 2024, MNRAS, 533, 3708, doi: [10.1093/mnras/stae1982](https://doi.org/10.1093/mnras/stae1982)

Lu, T., Rein, H., Tamayo, D., et al. 2023, ApJ, 948, 41, doi: [10.3847/1538-4357/acc06d](https://doi.org/10.3847/1538-4357/acc06d)

Luger, R., & Barnes, R. 2015, Astrobiology, 15, 119, doi: [10.1089/ast.2014.1231](https://doi.org/10.1089/ast.2014.1231)

LUVOIR Team, T. 2019, The LUVOIR Mission concept study final report, <https://arxiv.org/abs/1912.06219>

Martínez-Rodríguez, H., Caballero, J. A., Cifuentes, C., Piro, A. L., & Barnes, R. 2019, ApJ, 887, 261, doi: [10.3847/1538-4357/ab5640](https://doi.org/10.3847/1538-4357/ab5640)

Millholland, S. C., & Winn, J. N. 2025, Proceedings of the National Academy of Sciences, 122, e2416189122, doi: [10.1073/pnas.2416189122](https://doi.org/10.1073/pnas.2416189122)

Mulders, G. D., Pascucci, I., & Apai, D. 2015, ApJ, 814, 130, doi: [10.1088/0004-637X/814/2/130](https://doi.org/10.1088/0004-637X/814/2/130)

National Academies of Sciences, E. 2021, Pathways to discovery in astronomy and astrophysics for the 2020s, doi: [10.17226/26141](https://doi.org/10.17226/26141)

Neron de Surgy, O., & Laskar, J. 1997, A&A, 318, 975

Noyola, J. P., Satyal, S., & Musielak, Z. E. 2014, ApJ, 791, 25, doi: [10.1088/0004-637X/791/1/25](https://doi.org/10.1088/0004-637X/791/1/25)

Noyola, J. P., Satyal, S., & Musielak, Z. E. 2016, *ApJ*, 821, 97, doi: [10.3847/0004-637X/821/2/97](https://doi.org/10.3847/0004-637X/821/2/97)

Pass, E., Bean, J. L., Charbonneau, D., Cherubim, C., & Garcia-Mejia, J. 2024, A search for exoplanet satellites that are the same size as the Earth's moon,, JWST Proposal. Cycle 3, ID. #6193

Patel, S. D., Quarles, B., & Cuntz, M. 2025, *MNRAS*, 537, 2291, doi: [10.1093/mnras/staf131](https://doi.org/10.1093/mnras/staf131)

Patel, S. D., Quarles, B., Cuntz, M., & Weinberg, N. N. 2025, *Monthly Notices of the Royal Astronomical Society: Letters*, 542, L144, doi: [10.1093/mnrasl/slaf077](https://doi.org/10.1093/mnrasl/slaf077)

Pecaut, M. J., & Mamajek, E. E. 2013, *ApJS*, 208, 9, doi: [10.1088/0067-0049/208/1/9](https://doi.org/10.1088/0067-0049/208/1/9)

Piro, A. L. 2018, *AJ*, 156, 54, doi: [10.3847/1538-3881/aaaca38](https://doi.org/10.3847/1538-3881/aaaca38)

Ramirez, R. M. 2018, *Geosciences*, 8, 280, doi: [10.3390/geosciences8080280](https://doi.org/10.3390/geosciences8080280)

Ramirez, R. M., & Kaltenegger, L. 2014, *ApJL*, 797, L25, doi: [10.1088/2041-8205/797/2/L25](https://doi.org/10.1088/2041-8205/797/2/L25)

Rein, H., & Liu, S. F. 2012, *A&A*, 537, A128, doi: [10.1051/0004-6361/201118085](https://doi.org/10.1051/0004-6361/201118085)

Rein, H., & Spiegel, D. S. 2015, *MNRAS*, 446, 1424, doi: [10.1093/mnras/stu2164](https://doi.org/10.1093/mnras/stu2164)

Rosario-Franco, M., Quarles, B., Musielak, Z. E., & Cuntz, M. 2020, *AJ*, 159, 260, doi: [10.3847/1538-3881/ab89a7](https://doi.org/10.3847/1538-3881/ab89a7)

Sasaki, T., Barnes, J. W., & O'Brien, D. P. 2012, *ApJ*, 754, 51, doi: [10.1088/0004-637X/754/1/51](https://doi.org/10.1088/0004-637X/754/1/51)

Su, Y., & Saillenfest, M. 2025, arXiv e-prints, arXiv:2511.00161. <https://arxiv.org/abs/2511.00161>

Sullivan, III, W. T., & Baross, J. 2001, *Planets and Life* (Cambridge University Press)

Szabó, G. M., Schneider, J., Denes, Z., & Kálmán, S. 2024, *Universe*, 10, 110, doi: [10.3390/universe10030110](https://doi.org/10.3390/universe10030110)

Takaoka, K., Kuwahara, A., Ida, S., & Kurokawa, H. 2023, *A&A*, 674, A193, doi: [10.1051/0004-6361/202345915](https://doi.org/10.1051/0004-6361/202345915)

Tamayo, D., Rein, H., Shi, P., & Hernandez, D. M. 2020, *MNRAS*, 491, 2885, doi: [10.1093/mnras/stz2870](https://doi.org/10.1093/mnras/stz2870)

Teachey, A. 2024, arXiv e-prints, arXiv:2401.13293, doi: [10.48550/arXiv.2401.13293](https://doi.org/10.48550/arXiv.2401.13293)

Teachey, A., & Kipping, D. M. 2018, *Science Advances*, 4, eaav1784, doi: [10.1126/sciadv.aav1784](https://doi.org/10.1126/sciadv.aav1784)

Tinney, C. G., Butler, R. P., Marcy, G. W., et al. 2002, *ApJ*, 571, 528, doi: [10.1086/339916](https://doi.org/10.1086/339916)

Trifonov, T., Lee, M. H., Kürster, M., et al. 2020, *A&A*, 638, A16, doi: [10.1051/0004-6361/201936987](https://doi.org/10.1051/0004-6361/201936987)

Vanderburg, A., Rappaport, S. A., & Mayo, A. W. 2018, *AJ*, 156, 184, doi: [10.3847/1538-3881/aae0fc](https://doi.org/10.3847/1538-3881/aae0fc)

Wang, Y.-T., Liu, C., & Li, J. 2025, arXiv e-prints, arXiv:2506.12987, doi: [10.48550/arXiv.2506.12987](https://doi.org/10.48550/arXiv.2506.12987)

Williams, D. M., Kasting, J. F., & Wade, R. A. 1997, *Nature*, 385, 234, doi: [10.1038/385234a0](https://doi.org/10.1038/385234a0)

Zollinger, R. R., Armstrong, J. C., & Heller, R. 2017, *MNRAS*, 472, 8, doi: [10.1093/mnras/stx1861](https://doi.org/10.1093/mnras/stx1861)